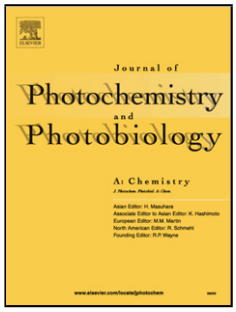

Title: Synergetic Effect of N^{3-}, In^{3+} and Sn^{4+} ions in TiO_2 towards Efficient Visible Photocatalysis

Authors: Zijian Lan, Yanlong Yu, Sai Yan, Enjun Wang, Jianghong Yao, Yaan Cao

PII: S1010-6030(17)31423-5
DOI: https://doi.org/10.1016/j.jphotochem.2017.12.032
Reference: JPC 11070

To appear in: *Journal of Photochemistry and Photobiology A: Chemistry*

Received date: 29-9-2017
Revised date: 9-12-2017
Accepted date: 22-12-2017

Please cite this article as: Zijian Lan, Yanlong Yu, Sai Yan, Enjun Wang, Jianghong Yao, Yaan Cao, Synergetic Effect of N3−, In3+ and Sn4+ ions in TiO2 towards Efficient Visible Photocatalysis, Journal of Photochemistry and Photobiology A: Chemistry https://doi.org/10.1016/j.jphotochem.2017.12.032

Synergetic Effect of N^{3-}, In^{3+} and Sn^{4+} ions in TiO_2 towards Efficient Visible Photocatalysis

Zijian Lan[a], Yanlong Yu[a], Sai Yan[a] , Enjun Wang[b], Jianghong Yao [a]* and Yaan Cao[a]*

[a] MOE Key Laboratory of Weak-Light Nonlinear Photonics, Ministry of Education, TEDA Applied Physics Institute and School of Physics, Nankai University, Tianjin 300457, China

[b] Hefei Institutes of Physical Science, Chinese Academy of Sciences, Hefei 230031, China

Graphical Abstract:

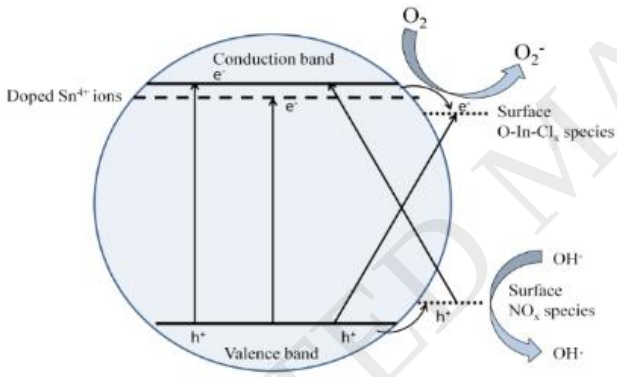

Highlights:

- the amount of charge carriers were increased significantly for TiO_2-N-In-Sn.
- TiO_2-N-In-Sn exhibit narrow band gap and strong response in visible region
- The TiO_2-N-In-Sn exhibit improved photocatalytic performance under visible irradiation

Abstract

Nitrogen, indium and tin doped TiO_2 photocatalyst (TiO_2-N-In-Sn) was prepared by sol-gel method. It is revealed that Sn ions were doped into TiO_2 lattice in substitutional mode, forming a new doped energy level 0.2 eV below the conduction band of TiO_2; nitrogen and indium ions are presented as surface NOx and O-In-Clx, located at 0.3 eV above the valence band and 0.3 eV below the conduction band, respectively. Owing to the synergetic effect of introduced nitrogen, indium and tin, the band structure of TiO_2 is adjusted to extend the visible absorption and promote the separation of charge carriers, resulting in an improved photocatalytic activity on photo-degradation of 4-CP under visible irradiation.

Keywords: Visible Photocatalysis; Surface Species; Band structure adjustment; TiO_2

1. Introduction

TiO_2 has been investigated widely as photocatalysts for solar energy conversion and environmental application, due to its great photocatalytic performance and chemical stability[1-5]. However, the photocatalytic application is still limited due to its high recombination efficiency of carriers and large band gap. Recent years, doping with metal and/or non-metal elements was regarded as one of the most efficient and effective methods for modification.[6-15] Among these, doping TiO_2 with nitrogen (TiO_2-N), tin (TiO_2-Sn) and indium (TiO_2-In) draws lots of attention. TiO_2-N shows enhanced visible photocatalytic activity owing to the narrowed band gap.[8, 9] Moreover, the doped Sn and In ions elements create new energy levels below the conduction band, enhancing the visible response and separating the charge carriers.[10, 16, 17] However, the amount of incorporated nitrogen is limited for practical application and it remains a huge challenge to

improve the visible photocatalytic performance of TiO_2. We are hoping to combine the advantages of Sn, In and N doped TiO_2 and adjust the band structure to extend the visible response, promote the separation of charge carriers and enhancing the photocatalytic performance under visible irradiaition.

In this work, a novel Sn, In and N doped TiO_2 photocatalyst was prepared by sol-gel method. The band structure is adjusted by introducing Sn, In and N into TiO_2 system, extending the visible response and inhibiting the recombination of charge carriers. The Sn, In and N tri-doped TiO_2 shows much better photocatalytic activity than the dole doped TiO_2. The enhanced photocatalytic mechanism as well as the synergetic effect of Sn, In and N ions is also discussed in details.

2. Experimental Details

2.1 Sample Preparation.

All chemicals used were of analytical grade and Milli-Q water (18.2 MΩ·cm) was used for all experiments. The tri-doped photocatalysts were synthesized by the steps as follow. First, solution A was prepared by mixing 3 mL of $InCl_3$ (0.6 mol L^{-1}) solution and 1 mL HCl solution (12 mol L^{-1}) with 40 mL ethanol at room temperature. Then 12 mL of $Ti(OC_4H_9)_4$ were added drop by drop to solution A under vigorous stirring. After completely mixing for 15 min, 0.2 mL $SnCl_4$ and 3 mL ammonia were added. The white precipitation was generated immediately and was aged at room temperature for 24 hours and dried at 373K, then annealed at 723K in a muffle for 2.5 hours. Pure TiO_2, nitrogen doped TiO_2 (TiO_2-N), indium doped TiO_2 (TiO_2-In) and tin doped TiO_2 (TiO_2-Sn) are prepared by the same procedure with corresponding reagent.

2.2 Characterization.

The XRD patterns were acquired on a Rigaku D/max 2500 X-ray diffraction spectrometer (Cu

Kα, λ=1.54056 Å). The average crystallite size was calculated according to the Scherrer formula ($D = k\,\lambda/B\cos\theta$). The BET surface areas of the samples were determined by nitrogen adsorption-desorption isotherm measurement at 77 K (Micromeritics Automatic Surface Area Analyzer Gemini 2360, Shimadzu). XPS measurements were carried out with an SECA Lab 220i-XL spectrometer by using an unmonochromated Al Kα (1486.6-eV) X-ray source and the spectra were calibrated to the binding energy of the adventitious C1s peak at 284.8 eV. The diffuse reflectance UV-visible absorption spectra were collected on a UV-visible spectrometer (U-4100, Hitachi). The photoluminescence (PL) spectra were measured by fluorescence spectrophotometer (Edinburgh Instruments, FLS920) using the 340 nm line of a Xe light as the excitation source.

2.3 Evaluation of Photocatalytic Activity.

The photocatalytic degradation of 4-chlorophenol (4-CP), a toxic pollutant with high stability under visible irradiation, was carried out in a 70 mL glass reactor with 10 mg amounts of catalysts suspended in 4-chlorophenol solution (5×10^{-5}mol L^{-1}, 40 mL, pH = 5.38) under visible irradiation and 5 mg amounts of catalysts suspended in 4-chlorophenol solution under UV irradiation. A sunlamp (Philips HPA 400/30S, Belgium) was used as light source. In order to achieve visible irradiation, a 400-nm filter was employed. The light beam was 10 cm away from the reactor perpendicularly. The 4-CP solution was continuously fed with O_2 gas (5 mL min^{-1}) under continuously stirring at 25 °C. The residual concentration of 4-chlorophenol was measured by a UV-visible spectrometer (UV-1061PC, SHIMADZU) every two hours, using 4-aminoantipyrine as the chromogenic reagent. Prior to photocatalytic reactions, the suspension was stirred in the dark for 30 min to reach the adsorption equilibrium of 4-chlorophenol.

3 Results and Discussion

Fig.1 shows the XRD of TiO_2, TiO_2-N, TiO_2-Sn, TiO_2-In and TiO_2-N-In-Sn. It can be clearly seen that anatase is the major phase and no other peaks, such as Ti_3N_4, In_2O_3 and SnO_2 are observed. Fig.2 shows the enlargement of (101) plane for anatase. Compared with pure TiO_2, no shift of the (101) peak is observable for TiO_2-N and TiO_2-In, while the (101) peak of TiO_2-Sn and TiO_2-N-In-Sn shifts to lower diffraction angles. The lattice parameters and cell volume are summarized in Table 1. Furthermore, the crystal size decreases after doping elements (Table 1), indicating doping nitrogen, indium and tin ions can inhibit the grain growth of TiO_2 particles remarkably. The BET specific surface area also ranks in the order of TiO_2<TiO_2-N< TiO_2- In< TiO_2-Sn <TiO_2-N-In-Sn (Table 1).

The corresponding lattice parameters and cell volume of TiO_2-N and TiO_2-In are almost the same as pure TiO_2, while those of TiO_2-Sn and TiO_2-N-In-Sn increase. Since the ionic radius of N is larger than that of O (N: 171 pm, O 140 pm)[18], N can hardly be weaved into TiO_2 in interstitial mode. Moreover, as the lattice parameters and cell volume did not change compared with pure TiO_2, that N are doped into TiO_2 lattice in substitutional mode can be excluded. As the ionic radius of In^{3+} ions (81 pm) is larger than Ti^{4+} ions (68 pm)[18], the lattice parameters and cell volume for TiO_2-In is expected, if In^{3+} ions are doped in substitutional mode. However, no changes are found for the lattice parameters and cell volume of TiO_2-In, suggesting In ions are not introduced into TiO_2 by substituting lattice Ti. Furthermore, an obvious increase in lattice parameters and cell volume is detected for TiO_2-Sn and TiO_2-N-In-Sn. Since the ionic radius of Sn^{4+} ions (71 pm) is larger than that of Ti^{4+} ions (68 pm), Sn ions are doped TiO_2 lattice by replacing Ti ions. Therefore, it can be concluded that Sn ions are doped in TiO_2 in substitutional mode, while indium and

nitrogen may exist as some surface species. The detailed existing states of N, In and Sn will be discussed by XPS.

As shown in Fig.3a, the XPS N 1s peak of TiO_2-N-In-Sn and TiO_2-N at about 400.1 eV is higher than that of Ti_3N_4 (396.9 eV), suggesting N atoms interact with O atoms[19, 20]. Therefore, the XPS peak at about 400.1 eV could be ascribed to the NO_X species on the surface of TiO_2[19, 20]. Fig.3b and 3c shows the In 3d and Cl 2p spectra of typical O-In-Cl_x (x=1 or 2) species which has been demonstrated by our previous work[10, 16, 18]. The binding energy of In $3d_{5/2}$ (445.2 eV) is between $InCl_3$ (446.0 eV) and In_2O_3 (444.6 eV) and that of Cl $2p_{3/2}$ locates between $TiCl_4$ and $InCl_3$[10, 16, 18], suggesting the introduced In^{3+} ions connect with unsaturated O^{2-} ions and Cl^- ions simultaneously, forming O-In-Cl_x (X=1 or 2) structure on TiO_2 surface. Fig.3d shows the Sn 3d spectra of TiO_2-N-In-Sn and TiO_2-Sn. The Sn $3d_{5/2}$ peak around 486.7 eV is between SnO_2(487.8 eV) and metallic Sn (485.0 eV), which is ascribed to the substitutional doped Sn ions.[11, 21, 22] Since the electronegativity of Sn (1.8) is larger than Ti (1.5), the electron density of Sn in Sn-O-Sn is higher than that in Sn-O-Ti. The corresponding binding energy of Sn^{4+} ions in substitutional mode is lower than that for SnO_2. Therefore, according to the XRD and XPS results, it can be concluded that In exists as O-In-Cl surface species, N forms NO_x species and Sn is doped into TiO_2 lattice in substitutional mode.

Fig.4 is the absorption of TiO_2, TiO_2-N, TiO_2-Sn, TiO_2-In and TiO_2-N-In-Sn. Pure TiO_2 exhibits strong absorption in UV region, attributed to the band-to-band transition. The on-set edge is about 410 nm, corresponding to a band gap of 3.02 eV. TiO_2-N shows small hump between 400 nm and 600 nm, ascribed to the electron transition from surface states of NO_x 0.3 eV above the valence band to the conduction band of TiO_2.[19, 20] A small hump from 400 nm to 500 nm is found for TiO_2-Sn, due to the electron transition from valence band to the energy levels of Sn ions 0.2 eV

below the conduction band. The strong absorption of TiO_2-In (450 nm - 700 nm) is attributed to electron transition from valence band to the energy levels of O-In-Cl_x species 0.3 eV below the conduction band. Furthermore, the TiO_2-N-In-Sn sample presents the strongest visible absorption among all samples, contributing from substitutional doped tin, the indium and nitrogen surface species. In addition, an obvious blue shift by 6 nm is found for TiO2-N-In-Sn sample and the corresponding band gap increases to 3.10 eV. The blue-shift is owing to the quantum size effect, indicating doping N, In and Sn elements into TiO_2 limit the grain growth of nanoparticles effectively and could be an efficient method for preparing visible photocatalysts.

Fig.5 shows the XPS valence band spectra of TiO_2, TiO_2-N, TiO_2-Sn, TiO_2-In and TiO_2-N-In-Sn samples. For pure TiO_2, the on-set edge (O 2p) is estimated to be 2.70 eV (+2.30 eV, vs NHE). Compared with TiO_2, the on-set edge for TiO_2-N, TiO_2-Sn, TiO_2-In and TiO_2-N-In-Sn are almost the same, suggesting the introduced Sn, In and N ion have no influence on the valence band of TiO_2.

To investigate the behavior of photogenerated carriers, Fig. 6 shows the photoluminescence spectra (PL) of TiO_2, TiO_2-N, TiO_2-Sn, TiO_2-In and TiO_2-N-In-Sn. The peaks at around 480 nm and 525 nm are attributed to the oxygen vacancies, located at 0.5 eV and 0.8 eV below the conduction band for TiO_2. Compared with pure TiO_2, the emission is slightly weakened for TiO_2-N, as the holes transferred to the NO_x species[18]. The peaks are further quenched for TiO_2-In and TiO_2-Sn, owing to the efficient trapping of surface O-In-Cl_x species and doped Sn ions. As we expect, the TiO_2-N-In-Sn sample shows the lowest PL intensity among all samples, suggesting the most efficient separation of charge carriers, arising from the doped Sn ions, surface NO_x species and O-In-Cl_x species. The electrons in the conduction band would also fall into the energy levels of O-In-Cl_x species and doped Sn ions other than the oxygen vacancies. The holes in the valence

band would move to the valence band to the energy levels of NO_x species. The photogenerated electrons and holes are separated more efficiently than the sole doped TiO_2 samples.

The photodegradation of 4-CP was applied to evaluate the catalytic activity of TiO_2, TiO_2-N, TiO_2-Sn, TiO_2-In and TiO_2-N-In-Sn, as shown in Fig.7. As shown in Fig.7a and Table 2, the 4-CP can hardly be degraded in the photolysis experiment after 8 hours' visible irradiation. Only a small amount of 4-CP was degraded for TiO_2. About 21.2%, 19.3% and 28.0% of 4-CP was degraded for TiO_2-N, TiO_2-Sn and TiO_2-In, respectively. For TiO_2-N-In-Sn sample, almost 90.7% of 4-CP was degraded, whose specific photocatalytic activity is about 4, 5 and 3 times higher than TiO_2-N, TiO_2-Sn and TiO_2-In, respectively. Under UV irradiation (Fig. 7b and Table 3), the TiO_2-N-In-Sn sample still exhibits a much better catalytic activity than TiO_2, TiO_2-N, TiO_2-Sn and TiO_2-In samples. These results suggest that doping In, Sn and N ions into TiO_2 system could improve the photocatalytic performance significantly under visible and UV irradiation.

Based on the discussion above, the reason why TiO_2-N-In-Sn exhibit the best photocatalytic activity on degradation of 4-CP could be explained via the mechanism scheme in Fig.8. Under visible irradiation, pure TiO_2 with a large band gap can hardly be excited, resulting in poor visible-light photocatalytic performance on degradation of 4-CP. After doping with nitrogen, the photo-generated electrons in the energy levels of NO_x surface species can be excited to the conduction band directly. Moreover, the NO_x species could also act as hole trapping centers, inhibiting the recombination of charge carriers. Thus, the photocatalytic performance of TiO_2-N is improved under visible light irradiation, compared with pure TiO_2. For TiO_2-In and TiO_2-Sn, electrons can be excited to the energy levels of O-In-Cl_x species or doped Sn ions, extending the visible response. Meanwhile, the electrons in the conduction band would fall into these energy levels, separating the charge carriers. More charge carriers would participate in the catalytic reaction, leading to

better catalytic activity than TiO_2. For TiO_2-N-In-Sn, electrons can be excited from the energy levels of NO_x species to the conduction band of TiO_2 or from the valence band to the energy levels of O-In-Cl_x species and doped Sn ions. The electrons in the conduction band would also fall into the energy levels of O-In-Cl_x species and doped Sn ions other than the oxygen vacancies. The photogenerated electrons and holes are separated more efficiently than the sole doped TiO_2 samples. Therefore, more charge carrier and generated and transfer to the surface of the photocatalyst. These electrons in the conduction band, energy levels of doped Sn ions and surface O-In-Cl_x species are trapped by the surface adsorbed O_2 molecules, forming O_2^- species which would further decompose the 4-CP. The holes in the valence band and energy levels of O-In-Cl_x species would oxidize the 4-CP molecules directly. As a result, TiO_2-N-In-Sn sample exhibit the best photocatalytic activity among all samples.

Under UV irradiation, electrons can be excited from the valence band to the conduction band directly for all samples. For TiO_2-N-In-Sn, the electrons in the conduction band can transfer to the energy levels of doped Sn ions or surface O-In-Cl_x species and the holes in the valence band can migrate to the surface energy levels of NO_x species, separating the charge carriers efficiently. Therefore, TiO_2-N-In-Sn sample presents an enhanced photocatalytic performance. Moreover, the enlarged band gap and increased surface area are also in favor of the photocatalytic activity for TiO_2-N-In-Sn. For the other sole doped TiO_2 (TiO_2-N, TiO_2-Sn, TiO_2-In), only part of process benefits the photocatalytic reaction, resulting in the limited photocatalytic performance.

Conclusion

A novel TiO_2 catalyst modified with In, Sn and N was prepared by sol-gel method. The band structure was adjusted by the introduction of In, Sn and N into TiO_2 system, so that the absorption was extended into visible region and more charge carriers were separated and participated in the

photocatalytic reaction. The TiO_2-N-In-Sn sample exhibited much better catalytic performance than TiO_2, TiO_2-N, TiO_2-Sn and TiO_2-In samples under visible and UV irradiation. The investigation about the synergetic effects of foreign elements would be helpful for developing TiO_2-based visible photocatalysts.

Acknowledgements

This work was supported by National Natural Science Foundation of China (no. 51372120) and China Postdoctoral Science Foundation (no. 2017M611149).

References

[1] A. Fujishima, K. Honda, Photolysis-Decomposition of Water at the Surface of an Irradiated Semiconductor, Nature, 238 (1972) 37-38.

[2] O. Khaselev, J.A. Turner, A Monolithic Photovoltaic-Photoelectrochemical Device for Hydrogen Production via Water Splitting, Science, 280 (1998) 425-427.

[3] S.U. Khan, M. Al-Shahry, W.B. Ingler, Efficient Photochemical Water Splitting by a Chemically Modified N-TiO2, Science, 297 (2002) 2243-2245.

[4] M.R. Hoffmann, S.T. Martin, W. Choi, D.W. Bahnemann, Environmental Applications of Semiconductor Photocatalysis, Chem. Rev., 95 (1995) 69-96.

[5] A. Hagfeldt, M. Graetzel, Light-Induced Redox Reactions in Nanocrystalline Systems, Chem. Rev., 95 (1995) 49-68.

[6] X. Li, F. Li, Study of Au/Au^{3+}-TiO_2 Photocatalysts Toward Visible Photooxidation for Water and Wastewater Treatment, Environ. Sci. Technol., 35 (2001) 2381-2387.

[7] M. Bowker, D. James, P. Stone, R. Bennett, N. Perkins, L. Millard, J. Greaves, A. Dickinson, Catalysis at the Metal-Support Interface: Exemplified by the Photocatalytic Reforming of Methanol on Pd/TiO_2, J. Catal., 217 (2003) 427-433.

[8] R. Asahi, T. Morikawa, T. Ohwaki, K. Aoki, Y. Taga, Visible-Light Photocatalysis in Nitrogen-Doped Titanium Oxides, Science, 293 (2001) 269-271.

[9] P.G. Wu, C.H. Ma, J.K. Shang, Effects of Nitrogen Doping on Optical Properties of TiO_2 Thin Films, Appl. Phys. A, 81 (2004) 1411-1417.

[10] Y. Yu, E. Wang, J. Yuan, Y. Cao, Enhanced Photocatalytic Activity of Titania with Unique Surface Indium and Boron Species, Appl. Surf. Sci., 273 (2013) 638-644.

[11] Y. Cao, T. He, L. Zhao, E. Wang, W. Yang, Y. Cao, Structure and Phase Transition Behavior of Sn^{4+}-Doped TiO_2 Nanoparticles, J. Phys. Chem. C, 113 (2009) 18121-18124.

[12] J. Yuan, E. Wang, Y. chen, W. Yang, J. Yao, Y. Cao, Doping Mode, Band Structure and Photocatalytic Mechanism of B-N-Codoped TiO_2, Appl. Surf. Sci., 257 (2011) 7355-7342.

[13] H. Pang, X. Li, Q. Zhao, H. Xue, W.-Y. Lai, Z. Hu, W. Huang, One-pot synthesis of heterogeneous Co 3 O 4-nanocube/Co (OH) 2-nanosheet hybrids for high-performance flexible asymmetric all-solid-state supercapacitors, Nano Energy, 35 (2017) 138-145.

[14] H. Pang, X. Li, S.Y. Ding, X. Xiao, J.Y. Shao, Y. Yu, J.L. Wei, N, S Co-doped 3D Mesoporous Carbon-Co3Si2O5 (OH) 4 Architectures for High-Performance Flexible Pseudo-Solid-State Supercapacitor, Journal of Materials Chemistry A, (2017).

[15] X. Li, H. Xue, H. Pang, Facile synthesis and shape evolution of well-defined phosphotungstic acid potassium nanocrystals as a highly efficient visible-light-driven photocatalyst, Nanoscale, 9 (2017) 216-222.

[16] E. Wang, W. Yang, Y. Cao, Unique Surface Chemical Species on Indium Doped TiO_2 and Their Effect on the Visible Light Photocatalytic Activity, J. Phys. Chem. C, 113 (2009) 20912-20917.

[17] H. Cao, S. Huang, Y. Yu, Y. Yan, Y. Lv, Y. Cao, Synthesis of TiO2-N/SnO2 heterostructure photocatalyst and its photocatalytic mechanism, J. Colloid Interface Sci., 486 (2017) 176-183.

[18] E. Wang, P. Zhang, Y. Chen, Z. Liu, T. He, Y. Cao, Improved Visible-Light Photocatalytic Activity of Titania Activated by Nitrogen and Indium Modification, J. Mater. Chem., 22 (2012) 14443-14449.

[19] P. Zhang, Y. Yu, E. Wang, J. Wang, J. Yao, Y. Cao, Structure of nitrogen and zirconium co-doped titania with enhanced visible-light photocatalytic activity, ACS Appl. Mater. Interfaces, 6 (2014) 4622-4629.

[20] Y. Cao, Y. Yu, P. Zhang, L. Zhang, T. He, Y. Cao, An Enhanced Visible-Light Photocatalytic Activity of TiO_2 by Nitrogen and Nickel–Chlorine Modification, Sep. Purif. Technol., 104 (2013) 256-262.

[21] C. Han, S. Huang, Y. Yu, Y. Yan, Y. Lv, Y. Cao, Synthesis of TiO 2 -N/SnO 2 heterostructure photocatalyst and its photocatalytic mechanism, J. Colloid Interface Sci., 486 (2017) 176-183.

[22] Y. Cao, T. He, Y. Chen, Y. Cao, Fabrication of Rutile TiO_2−Sn/Anatase TiO_2−N Heterostructure and Its Application in Visible-Light Photocatalysis, J. Phys. Chem. C, 114 (2010) 3627-3633.

Figure captions

Fig. 1 XRD patterns of TiO_2 (a), TiO_2-N (b), TiO_2-In (c), TiO_2-Sn (d) and TiO_2-N-In-Sn (e).

Fig. 2 The enlarged XRD peaks of crystal plane (1 0 1) of TiO_2 (a), TiO_2-N (b), TiO_2-In (c), TiO_2-Sn (d) and TiO_2-N-In-Sn (e).

Fig. 3(a) XPS spectra of N1s, (b) In3d, (c) Cl2p and (d) Sn3d for TiO_2-N-In-Sn sample and corresponding samples.

Fig. 4 Diffuse reflectance absorption spectra of (a) pure TiO_2, (b) N -TiO_2, (c) Sn-TiO_2, (d) In-TiO_2 and (e) TiO_2-N-In-Sn.

Fig. 5 XPS valence band spectra of TiO_2, TiO_2-N, TiO_2-In, TiO_2-Sn and TiO_2-N-In-Sn samples.

Fig. 6 Photoluminescence spectra of pure TiO_2, TiO_2-N, TiO_2-N-In and TiO_2-N-In-Sn.

Fig. 7 Temporal course of the photodegradation of 4-CP under visible light (left) irradiation and UV irradiation (right): (a) pure TiO_2, (b) N -TiO_2, (c) Sn-TiO_2, (d) In-TiO_2 and (e) TiO_2-N-In-Sn.

Fig. 8 Schematic diagram of photocatalytic mechanism for nitrogen and indium co-doped TiO_2.

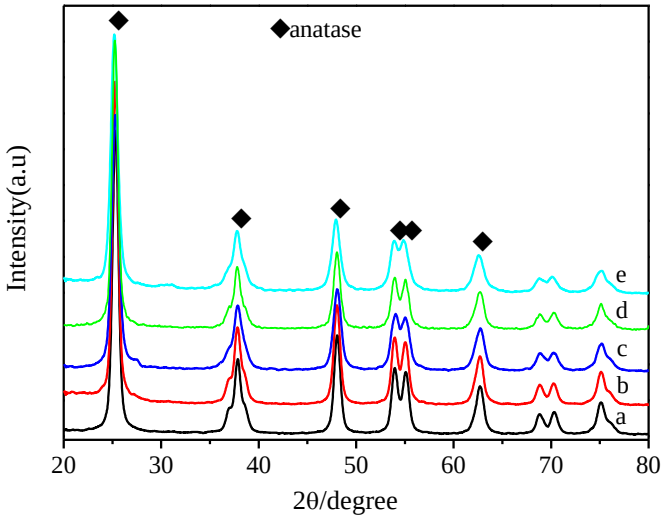

Fig. 1 XRD patterns of TiO_2 (a), TiO_2-N (b), TiO_2-In (c), TiO_2-Sn (d) and TiO_2-N-In-Sn (e).

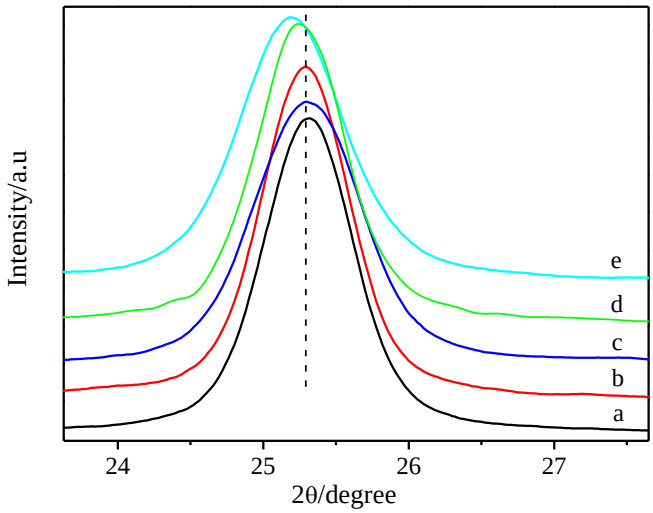

Fig. 2 The enlarged XRD peaks of crystal plane (1 0 1) of TiO_2 (a), TiO_2-N (b), TiO_2-In (c), TiO_2-Sn (d) and TiO_2-N-In-Sn (e).

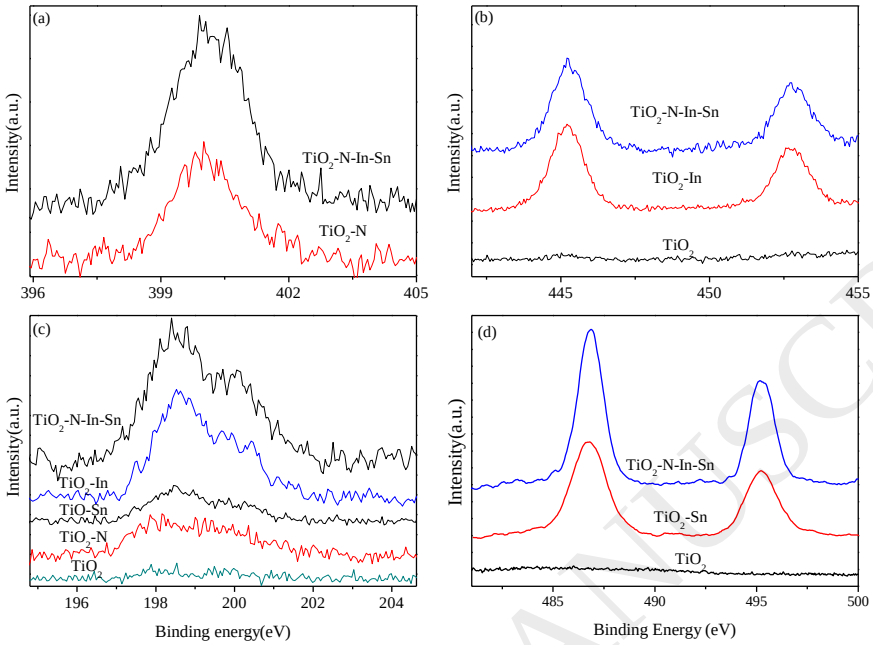

Fig. 3 (a) XPS spectra of N1s, (b) In3d, (c) Cl2p and (d) Sn3d for TiO_2-N-In-Sn sample and corresponding samples.

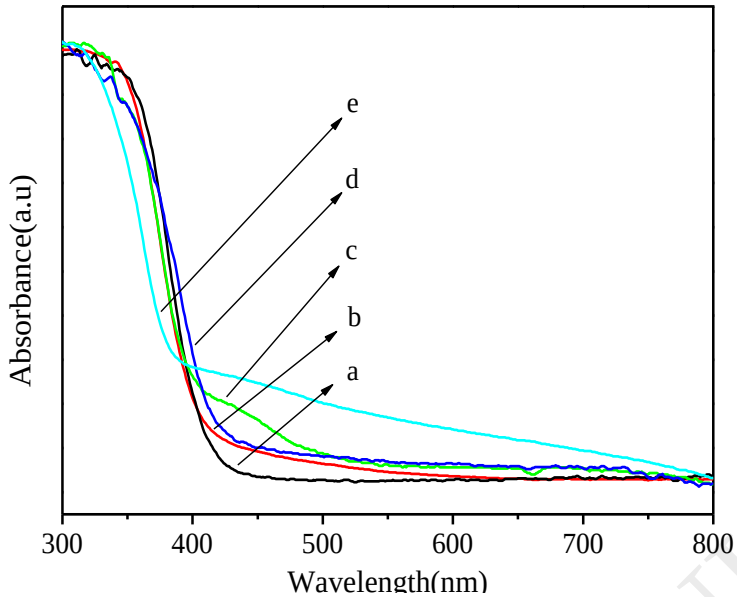

Fig. 4 Diffuse reflectance absorption spectra of (a) pure TiO_2, (b) N -TiO_2, (c) Sn-TiO_2, (d) In-TiO_2 and (e) TiO_2-N-In-Sn.

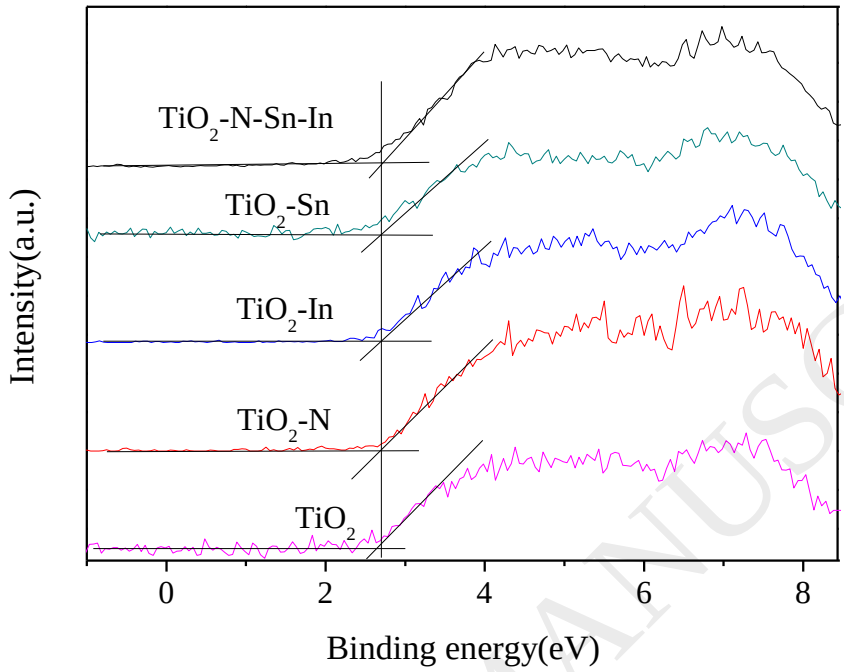

Fig. 5 XPS valence band spectra of TiO_2, TiO_2-N, TiO_2-In, TiO_2-Sn and TiO_2-N-In-Sn samples.

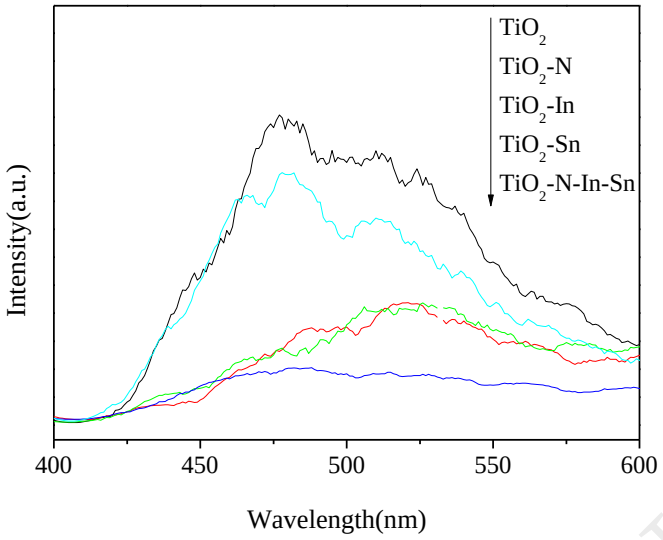

Fig. 6 Photoluminescence spectra of pure TiO_2, TiO_2-N, TiO_2-N-In and TiO_2-N-In-Sn.

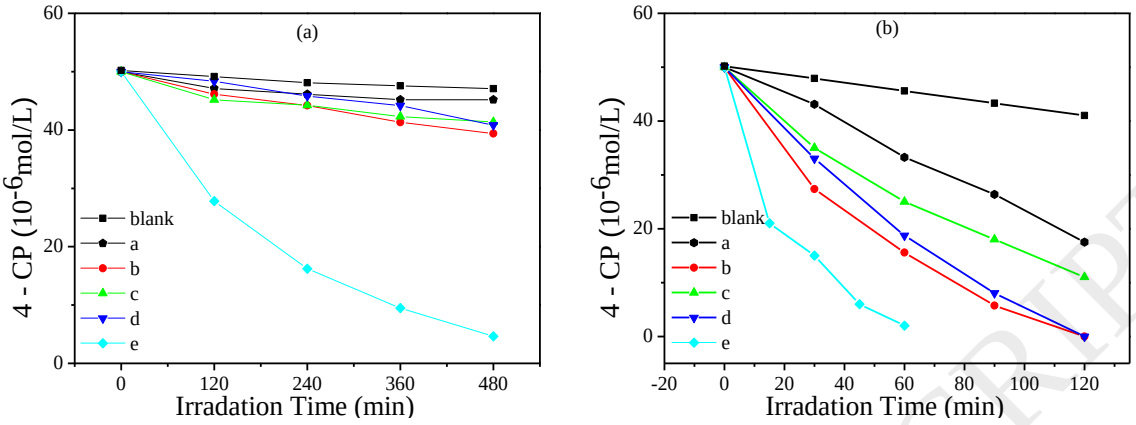

Fig. 7 Temporal course of the photodegradation of 4-CP (5.0×10^{-5} mol L^{-1}; 40 mL) in aqueous dispersions containing 10 mg of catalysts under visible light (left) irradiation and 5 mg under UV irradiation (right): (a) pure TiO_2, (b) N -TiO_2, (c) Sn-TiO_2, (d) In-TiO_2 and (e) TiO_2-N-In-Sn.

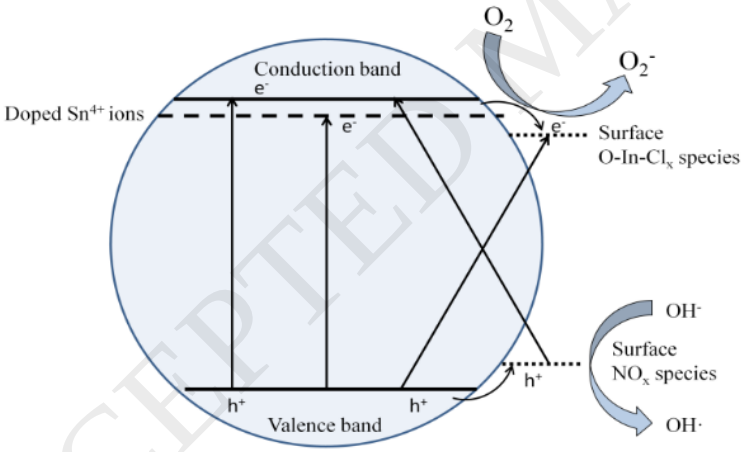

Fig. 8 Schematic diagram of photocatalytic mechanism for nitrogen, tin and indium co-doped TiO_2.

Tables

Table 1. The phases, crystallite sizes and surface areas of pure TiO_2 and TiO_2-N, TiO_2-Sn, TiO_2-In and TiO_2-N-In-Sn.

sample	cell parameters (Å)		cell volume ($Å^3$)	crystallite size (nm)	S_{BET} ($m^2\ g^{-1}$)
	a =*b*	*c*			
TiO_2	3.784	9.501	136.03	12	68
TiO_2-N	3.786	9.497	136.16	12	76
TiO_2-Sn	3.794	9.487	136.57	8	112
TiO_2-In	3.785	9.489	135.97	9	82
TiO_2-N-In-Sn	3.795	9.508	136.97	9	114

Table 2 The photodegradation of 4-CP under visible light irradiation (λ>400nm).

Sample	Degradation ratio[a]($\Delta c/c_0$)	k [b]/min^{-1}	$t_{1/2}$/min	Specific photocatalytic activity /($mol \cdot g^{-1} \cdot h^{-1}$)
Blank [c]	0.035	7.42×10^{-5}	9338.7	—
TiO_2	0.097	2.11×10^{-4}	3275.0	2.42×10^{-6}
TiO_2-N	0.212	4.97×10^{-4}	1393.5	5.30×10^{-6}
TiO_2-Sn	0.193	4.71×10^{-4}	1469.4	4.82×10^{-6}
TiO_2-In	0.280	6.84×10^{-4}	1012.8	7.00×10^{-6}
TiO_2-N-In-Sn	0.907	4.95×10^{-3}	140.0	2.27×10^{-5}

[a] After reaction for 8 h. [b] Apparent rate constant deduced from the linear fitting of $\ln(c_0/c)$ versus reaction time. [c] The blank was the photolysis of 4-CP.

Table 3. The photodegradation of 4-CP under UV light irradiation.

Sample	Degradation ratio[a]($\Delta c/c_0$)	k [b]/min^{-1}	$t_{1/2}$/min	Specific photocatalytic activity /($mol \cdot g^{-1} \cdot h^{-1}$)
Blank [c]	0.043	7.25×10^{-4}	955.3	—
TiO_2	0.335	6.79×10^{-3}	102.1	1.34×10^{-4}
TiO_2-N	0.689	3.84×10^{-2}	18.1	2.76×10^{-4}
TiO_2-Sn	0.500	2.79×10^{-2}	24.8	2.00×10^{-4}
TiO_2-In	0.625	3.49×10^{-2}	19.8	2.50×10^{-4}
TiO_2-N-In-Sn	0.960	5.36×10^{-2}	12.9	3.84×10^{-4}

[a] After reaction for 1 h. [b] Apparent rate constant deduced from the linear fitting of $ln(c_0/c)$ versus reaction time. [c] The blank was the photolysis of 4-CP